Heliyon 10 (2024) e26286

Contents lists available at ScienceDirect

Heliyon

journal homepage: www.cell.com/heliyon

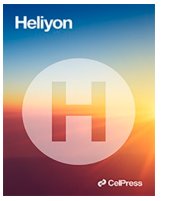

Research article

$TiFe_2O_4$@SiO_2–SO_3H: A novel and effective catalyst for esterification reaction

Mohanad Yakdhan Saleh [a], Ahmed Kareem Obaid Aldulaimi [b,*], Shakir Mahmood Saeed [c], Ayat Hussein Adhab [d]

[a] Department of Chemistry, College of Education for Pure Science, University of Mosul, Mosul, Iraq
[b] College of Food Sciences, Al-Qasim Green University, Babylon, Iraq
[c] Department of Pharmacy, Al-Noor University College, Nineveh, Iraq
[d] Department of Pharmacy, Al-Zahrawi University College, Karbala, Iraq

ARTICLE INFO

Keywords:
$TiFe_2O_4$
Palmitic acid
SO_3H
Catalyst

ABSTRACT

In the present study, $TiFe_2O_4$@SiO_2–SO_3H heterogeneous catalyst was successfully synthesized and applied to generate biodiesel from oleic acid, and palmitic acid using an esterification process. In this sense, the nanocatalyst surface was characterized using TEM, TGA, XRD, FTIR, VSM, BET, SEM, and EDX analyses. Nanocatalyst $TiFe_2O_4$@SiO_2–SO_3H showed high activity for the esterification of oleic acid and palmitic acid. Also, the nanocatalyst can be easily recovered with a bar magnet and reused many times without any loss of activity.

1. Introduction

Esterification of alcohols with carboxylic acids has recently attracted the attention of scientists for the industrial production of useful chemicals such as perfumes, biodiesel, polymers, solvents, etc. [1–4]. In the next decade, due to the reduction of non-renewable fossil fuels and energy consumption, biodiesel will be a suitable alternative in the industry [5] [–] [8]. Biodiesel is a renewable, clean, sulfur-free, and sustainable fuel derived from monoalkyl esters of fatty acids. Biodiesel is usually produced by the esterification of fatty acids in non-edible or edible oils with primary alcohols using basic or acidic catalysts [9,10]. Also, esterification of free fatty acids such as palmitic acid and oleic acid in incompatible raw materials before using basic catalysts is important for the transesterification reaction due to soap formation, therefore acid nanocatalysis is more suitable for biodiesel production [11]. Therefore, using an acid catalyst, environmentally friendly and green biodiesel can be produced from palmitic acid and oleic acid [12,13].

The development and research of green and efficient nanomaterials as catalyst supports is a big challenge in the synthesis of organic compounds [14] [–] [16]. In the last decade, magnetic nanoparticles have been recognized as excellent supports due to their easy preparation and operation, and high surface area, easy recovery by the magnetic field, which will lead to increased product purity [17, 18]. Also, the most important advantage of magnetic nanoparticles is their separation from the reaction mixture with the help of a bar magnet [19]. Among the heterogeneous nanocatalysts, $TiFe_2O_4$ has received much attention due to its simplicity in the synthesis method and easy separation using magnets [20,21]. However, various catalysts can be supported on $TiFe_2O_4$ nanoparticles, because they can be easily separated after several consecutive uses in the reaction [22,23].

In this work, we report the synthesis and structural characterization of a green and novel catalyst and investigate their utility as a

* Corresponding author.
E-mail address: ahmedaldulaimi1@gmail.com (A.K. Obaid Aldulaimi).

https://doi.org/10.1016/j.heliyon.2024.e26286
Received 6 November 2023; Received in revised form 30 January 2024; Accepted 9 February 2024
Available online 10 February 2024

green and efficient catalyst in Biodiesel Production. Compared to previously reported catalysts, this solid acid catalyst showed better catalytic performance.

2. Experimental

2.1. Preparation of $TiFe_2O_4@SiO_2–SO_3H$

To synthesize the $TiFe_2O_4$ NPs, 10 mmol of Titanium isopropoxide ($C_{12}H_{28}O_4Ti$) and 20 mmol of $FeCl_3.4H_2O$ were prepared and the mixture was maintained at 70 °C water bath for 30 min. Next, 5 g of sodium hydroxide was added and the mixture was stirred. The resulting particles were harvested, washed several times using H_2O, and dried at 100 °C (Scheme 1). Next, 2.0 g of the obtained $TiFe_2O_4$ was dispersed in a mixture of ethanol (70 mL), 10.0 mL of ammonia solution, 20 mL of H_2O, followed by the addition of 5 g of PEG, and 2.5 mL of TEOS (tetraethyl orthosilicate). This solution was stirred for 24 h at room temperature. Also, the product ($TiFe_2O_4@SiO_2$) was separated using a simple magnet washed several times with ethanol and water, and dried at room temperature. Finally, to prepare the $TiFe_2O_4@SiO_2–SO_3H$ catalyst, a mixture of $TiFe_2O_4@SiO_2$ (2.0 g) was dispersed in 100 ml of hexane in a round-bottomed flask. In the next step, 0.3 g of chlorosulfonic acid was added drop by drop to the reaction vessel and finally stirred at 25 °C for 24 h. Next, after completion of the reaction, the final catalyst ($TiFe_2O_4@SiO_2–SO_3H$) was separated and washed with H_2O and ethanol and, dried under vacuum at 55 °C (Scheme 1).

2.2. Biodiesel production

The catalytic activity of $TiFe_2O_4@SiO_2–SO_3H$ was used for the esterification reactions of oleic acid. Therefore, methanol (9 mmol), oil (2 mmol), and nanocatalyst (0.02 g) were mixed in a round-bottom flask. Afterward, the mixture was heated at 60 °C for 1.5 h. The nanocatalyst was separated using a magnet after the completion of the reaction, and excess methanol was removed from the upper liquid phase using rotary evaporation. The extracted organic phase was washed with distilled water to remove the remaining impurities and finally, sodium sulfate was used to dry the organic phase (Scheme 2).

The catalytic activity of $TiFe_2O_4@SiO_2–SO_3H$ was used for esterification reactions of Palmitic acid. Therefore, Palmitic acid (2 mmol), methanol (9 mmol), and $TiFe_2O_4@SiO_2–SO_3H$ (catalyst) (0.02 g) were mixed in a round-bottom flask (Scheme 3). Afterward, the mixture was heated at 70 °C for 1 h. After the completion of the reaction, $TiFe_2O_4@SiO_2–SO_3H$ was separated using an external magnet, and excess methanol was removed from the upper liquid phase using rotary evaporation. Then, to remove impurities, the organic phase was washed with distilled water and dried using Na_2SO_4.

2.3. Selected NMR data

S_1) Methyl oleate: ^{1}H NMR ($CDCl_3$, 400 MHz): δ = 0.83 (s, 3H, CH_3), 1.11 (m, 20H, $10CH_2$), 1.36 (m, 2H, CH_2), 1.89 (m, 4H, $2CH_2$), 2.35 (t, 2H, CH_2), 3.56 (s, 3H, CH_3), 5.59 (m, 2H, 2CH) ppm. FT-IR (KBr) cm^{-1}: 589, 720, 1202, 1463, 1752, 2953.

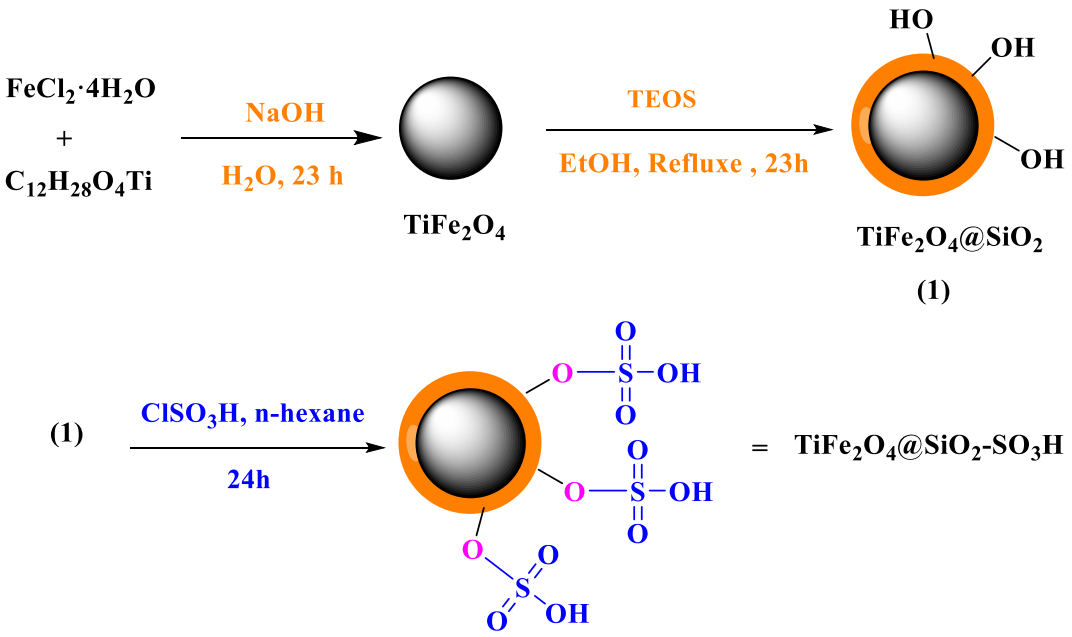

Scheme 1. Synthesis of $TiFe_2O_4@SiO_2–SO_3H$

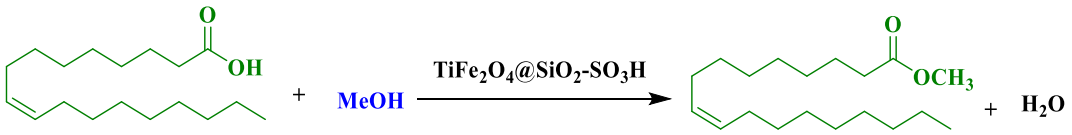

Scheme 2. Esterification of oleic acid.

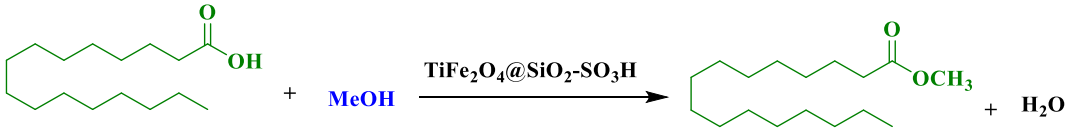

Scheme 3. Esterification of Palmitic acid.

S_2) methyl palmitate:^{1}H NMR ($CDCl_3$, 400 MHz): δ = 0.83 (s, 3H, CH_3), 1.03 (m, 24H, 12CH_2), 1.49 (m, 2H, CH_2), 2.19 (m, 2H, CH_2), 4.15 (s, 3H, CH_3) ppm. FT-IR (KBr) cm^{-1}: 604, 723, 1208, 1743, 2884, 3426.

2.3.1. Catalyst characterizations

FT-IR spectra of $TiFe_2O_4$ (a), $TiFe_2O_4$@SiO_2 (b), and $TiFe_2O_4$@SiO_2–SO_3H (c) catalyst are shown in Fig. 1. The FT-IR spectrum of $TiFe_2O_4$ nanoparticles shows two bands in the regions of 505 and 648 cm^{-1} are assigned to the stretching vibrations of the titanium–oxygen and the iron-oxygen bonds, respectively. In Fig. 1b, the observation of the stretching vibration band at 1106 cm^{-1} is related to Si–O bonds and evidence for the presence of SiO_2 on the surface of $TiFe_2O_4$ nanoparticles. In Fig. 1c, the functionalization of –SO_3H groups on $TiFe_2O_4$@SiO_2 was approved by the absorption of OH stretching bands of the –SO_3H moiety at 2500–3500 cm-1 in the FT-IR spectrum [24].

Fig. 2 shows the FT-IR spectrum of the nanocatalyst after recycling. There is no change in the FT-IR of $TiFe_2O_4$@SiO_2–SO_3H after recovery, which confirms the stability of the nanocatalyst (Fig. 2).

The XRD pattern of $TiFe_2O_4$@SiO_2–SO_3H nanocomposite was presented in Fig. 3a and b. As shown in Fig. 3a, the $TiFe_2O_4$@-SiO_2–SO_3H MNPs afforded seven sharp and strong peaks at 2θ = 30.1, 35.45, 43.12, 53.27, 56.88 and 62.45 indexed to the (2 2 0), (3 1 1), (4 0 0), (4 2 2), (5 1 1) and (4 4 0) planes, respectively showing good agreement with XRD pattern of previous reports on $TiFe_2O_4$ MNPs. These analyzes confirm that the $TiFe_2O_4$ structure is not degraded by the silica sulfuric acid shell stabilization, and that the background noise is caused by the dried amorphous SO_3H shells (Fig. 3b) [25].

The TGA was investigated for the quantitative determination of the ligand (SiO_2–SO_3H) supported on the surface of $TiFe_2O_4$ magnetic nanoparticles (Fig. 4). As illustrated in Fig. 4a, the curve of $TiFe_2O_4$, the first change which is observed below 200 °C may have corresponded to the loss of physically adsorbed H_2O on the surface of this compound. The little quantity of weight loss (6%) after 200 °C is due to the removal of SiO_2 groups (Fig. 4b). As shown in Fig. 4c, for $TiFe_2O_4$@SiO_2–SO_3H, there is a weight loss of 11% between 250 and 700 °C related to the breakdown of the $TiFe_2O_4$@SiO_2–SO_3H moieties. The results of the TGA analysis confirmed the successful support of SiO_2–SO_3H on the surface of $TiFe_2O_4$ MNPs.

The EDX image of $TiFe_2O_4$@SiO_2–SO_3H nanocatalyst (Fig. 5) shows the presence of Ti, Si, Fe, S, and O elements. These results show that there are no other impurities related to the solvents and materials used in the catalyst synthesis steps.

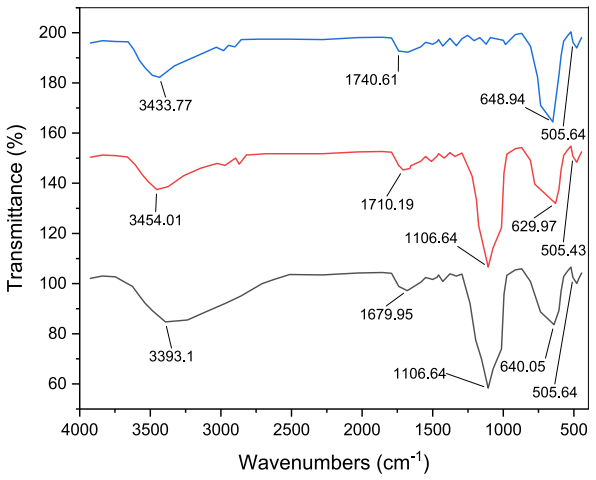

Fig. 1. Comparative study of FTIR spectra of a) $TiFe_2O_4$, b) $TiFe_2O_4$@SiO_2, c) $TiFe_2O_4$@SiO_2–SO_3H

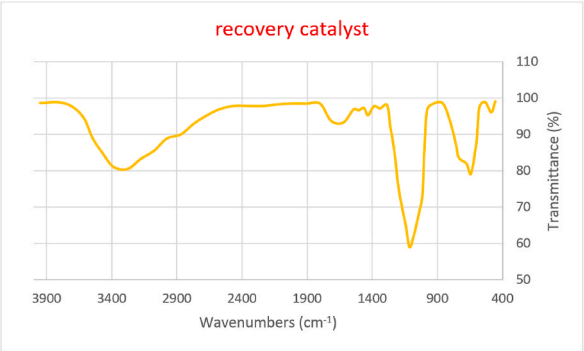

Fig. 2. FTIR spectra of recovery $TiFe_2O_4@SiO_2–SO_3H$

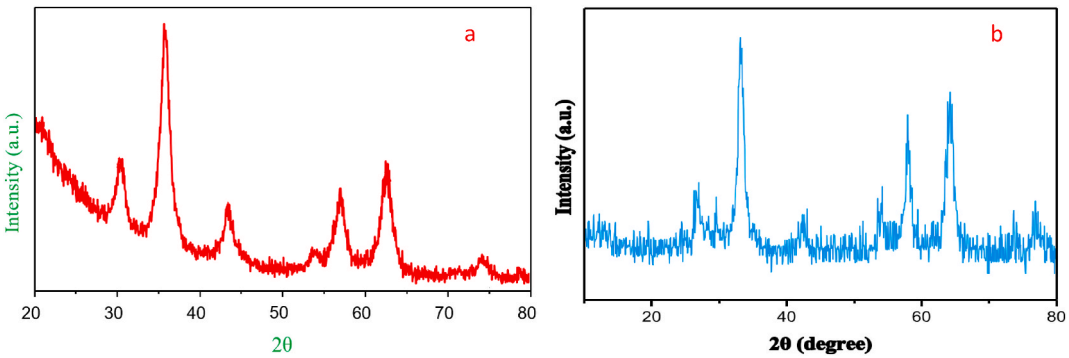

Fig. 3. XRD spectrum of a) $TiFe_2O_4$ and b) $TiFe_2O_4@SiO_2–SO_3H$

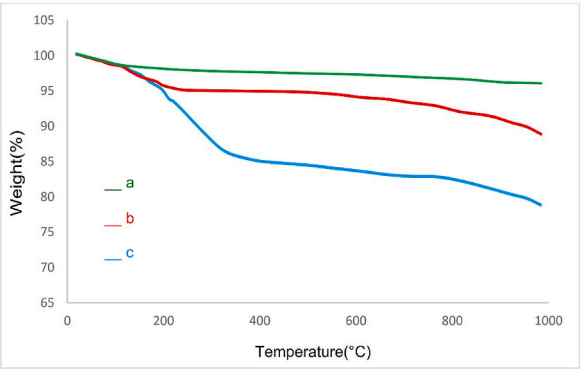

Fig. 4. TGA curve of a) $TiFe_2O_4$, b) $TiFe_2O_4@SiO_2$, c) $TiFe_2O_4@SiO_2–SO_3H$.

The morphology of the nanoparticles in the scanning electron microscope (SEM) images (Fig. 6) shows that the nanoparticles are spherical and have a relatively uniform distribution. The SEM images of $TiFe_2O_4$ (Fig. 6a, b, and 6c) and $TiFe_2O_4@SiO_2–SO_3H$ (Fig. 6d, e, and 6f) declared that the catalyst was synthesized as nanometer-sized quasi-spherical particles with 60–100 nm average diameter (Fig. 6). Also, a continuous layer of the $SiO_2–SO_3H$ can be observed on the surface of the catalyst, if we compare $TiFe_2O_4@SiO_2–SO_3H$ result with $TiFe_2O_4$.

$TiFe_2O_4$ (Fig. 7a and b) and $TiFe_2O_4@SiO_2–SO_3H$ (Fig. 7c and d) were characterized by TEM. The scanning electron microscopy images show that the size of the nanocatalyst particles is in the nanometer range (60–100 nm) with a sphere-like structure. Transmission electron microscopy images confirmed these observations (Fig. 7).

The adsorption–desorption isotherms of N_2 at 77 K were characterized by porosity adsorption (Fig. 8). BET analysis was performed to know the mean pore diameter, total pore volume, and surface area of $TiFe_2O_4$ and $TiFe_2O_4@SiO_2–SO_3H$. In Fig. 8a, the N_2 adsorption–desorption isotherm of $TiFe_2O_4$ has been displayed. Regarding the N_2 adsorption-desorption isotherms technique, the obtained surface area of $TiFe_2O_4$ is 100.39 (m^2/g). As shown in Fig. 8a, the size distribution and pore volumes of $TiFe_2O_4$ obtained

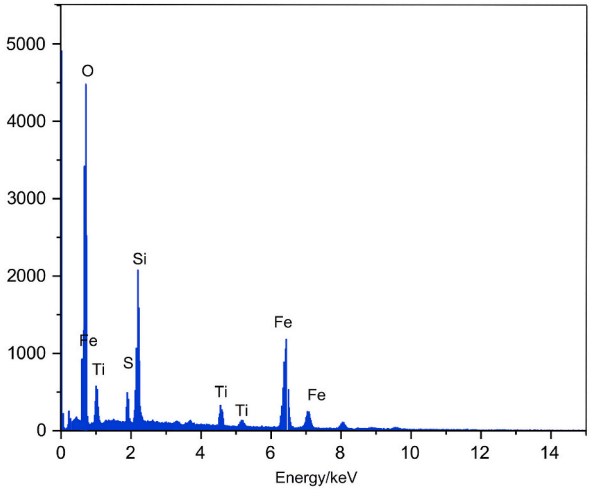

Fig. 5. EDX images of $TiFe_2O_4@SiO_2–SO_3H$.

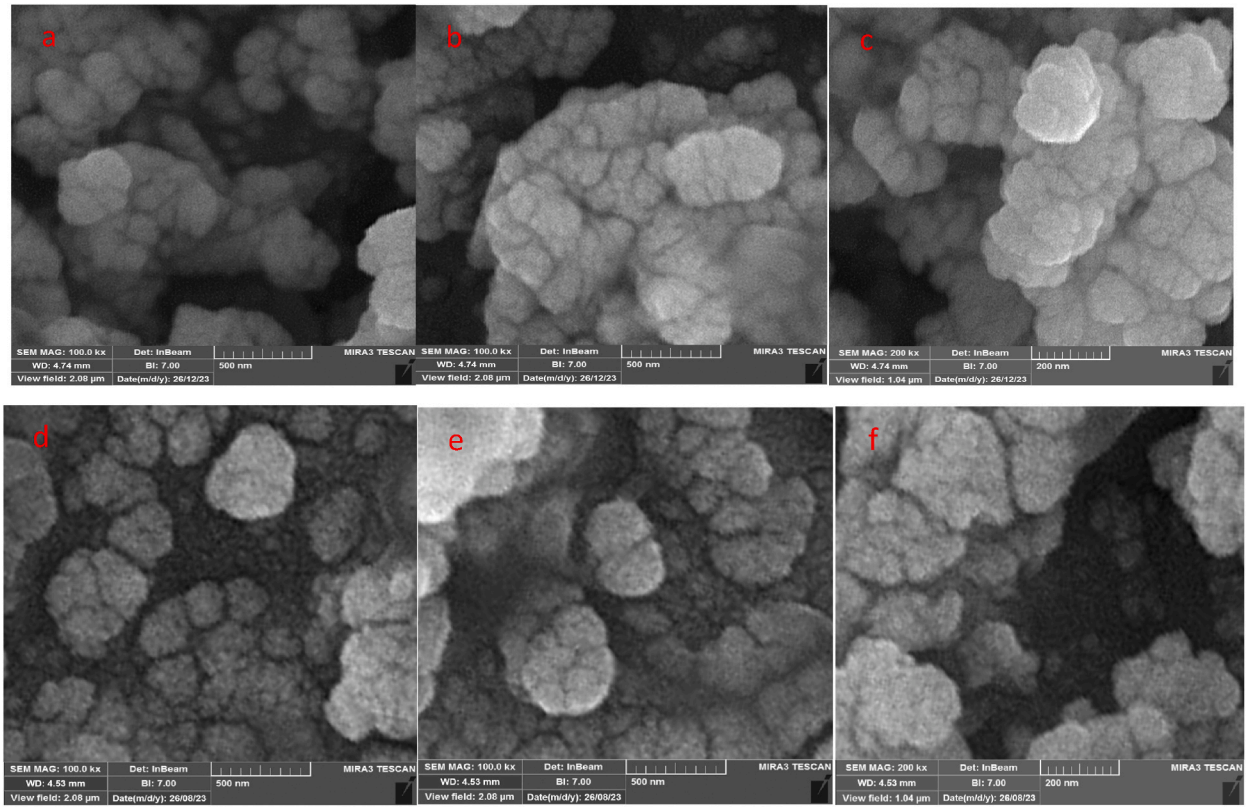

Fig. 6. SEM images of $TiFe_2O_4$ (a–c), $TiFe_2O_4@SiO_2–SO_3H$ (d–f).

were 0.34 $cm^3\ g^{-1}$ and 5.7 nm respectively. Also, in Fig. 8b, the N_2 adsorption–desorption isotherm of $TiFe_2O_4@SiO_2–SO_3H$ can be observed. Regarding the N_2 adsorption-desorption isotherms, based on the BET method, the obtained surface area of $TiFe_2O_4@SiO_2–SO_3H$ is 21.01 (m^2/g). Also, the total pore volumes and mean pore diameter of $TiFe_2O_4@SiO_2–SO_3H$ were 0.15 $cm^3\ g^{-1}$, and 16 nm, respectively. The reduction of the surface area in the final catalyst is due to the successful fixation of SO_3H on the surface of $TiFe_2O_4$ (Fig. 8a and b).

In the next step, using the back-titration method, the acid strength of the synthesized catalyst, that is, the surface density of SO_3H groups, was determined. First, 0.1 g of the synthesized catalyst was dispersed in 60 ml of water in a flask and stirred for 30 min, then 10 ml of NaOH (0.1 N) was added to the reaction vessel under constant stirring and until the pH changed. did not change. The catalyst was

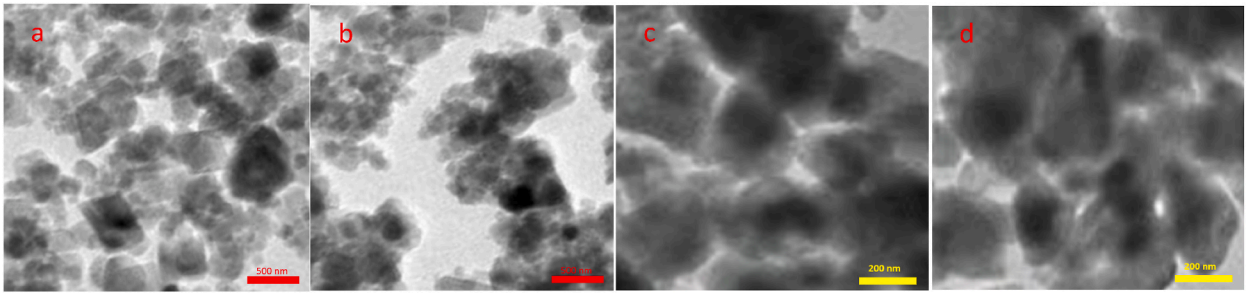

Fig. 7. TEM images of $TiFe_2O_4$ (a and b), and $TiFe_2O_4$@SiO_2–SO_3H (c and d).

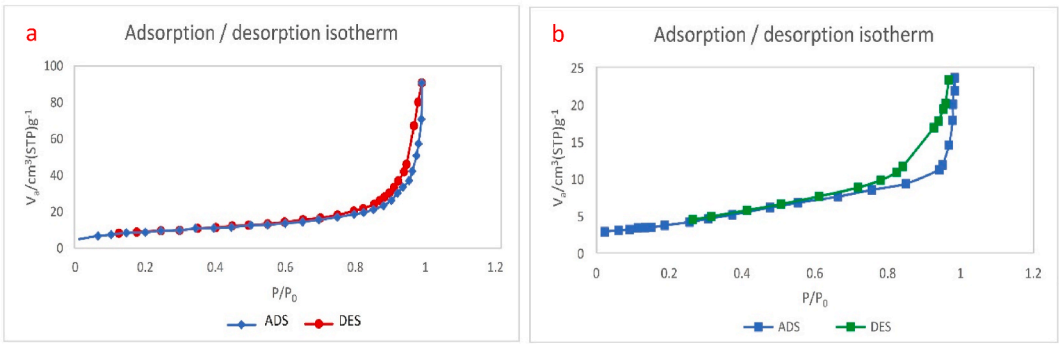

Fig. 8. Nitrogen adsorption-desorption isotherm for $TiFe_2O_4$ (a) and $TiFe_2O_4$@SiO_2–SO_3H (b).

separated using an external magnet. Then, two drops of phenolphthalein were added to the container and were tittered with 1.1 ml HCl (0.1 N). Thus 1 g of catalyst has 8.9 mmol of the acidic group which is higher than the amount reported so far in the literature.

The magnetic property of the catalyst was investigated by VSM analysis and its results are shown in Fig. 9. The value of saturation magnetism (Ms) for the catalyst is 5.51 emu/g. However, the synthesized catalyst was easily separated from the reaction mixture by an external magnet.

2.3.2. *Catalytic studies*

2.3.2.1. Esterification reactions. Next, the catalytic activity of $TiFe_2O_4$@SiO_2–SO_3H was investigated using the esterification of methanol with oleic acid. To optimize the reaction conditions in the presence of $TiFe_2O_4$@SiO_2–SO_3H for biodiesel production, the effect of various parameters such as the amount of catalyst (0.03–0.007 g), molar ratios of methanol to oleic acid, base, and temperature were investigated. By using 0.02 g of the reported nanocatalyst, the maximum production of biodiesel was obtained. A maximum conversion of 97 % (oleic acid to ester) was achieved for the temperature of 60 °C. The molar ratio between oil and methanol was considered to be 9:2 in this study for the completion of the esterification process. The excess amount of alcohol in the esterification of fatty acids will help to disperse the catalyst in the reaction media, leading to more biodiesel production. Also, excess alcohol prevents the reverse reaction and, as in other esterification reactions, more ester is produced (Table 1).

Next, the catalytic activity of $TiFe_2O_4$@SiO_2–SO_3H was investigated using the esterification of palmitic acid with methanol (Table 2). The model reaction was carried out in the absence of a mesoporous catalyst ($TiFe_2O_4$@SiO_2–SO_3H) even after 5 h, there is no product was observed. Also, according to the obtained results, the reaction efficiency decreased with the decrease in the amount of nanocatalyst. The results are shown in Table 2.

The mechanism of $TiFe_2O_4$@SiO_2–SO_3H catalytic esterification is shown in Scheme 4. Initially, $TiFe_2O_4$@SiO_2–SO_3H acts as an acid catalyst to activate the carbonyl group of oleic acid to form positive carbon ions. The acidic $TiFe_2O_4$@SiO_2–SO_3H catalyst can provide H^+, and the H^+ attacks the carbonyl group of oleic acid. Then protonation of the carbonyl group leads to the generation of carbocation. In the end, after the nucleophilic attack of the methanol molecule, a tetrahedral intermediate is formed, Water molecules are removed, and finally biodiesel and H^+ will be produced.

2.3.2.2. Hot filtration. With optimal reaction conditions in hand (esterification reaction of Palmitic acid and MeOH), to test the heterogeneous nature of the $TiFe_2O_4$@SiO_2–SO_3H hot filtration experiment was performed under the optimal reaction conditions. In the absence of catalyst, the maximum yield was about 4% at 1h, showing that the reaction could not progress without an acid catalyst. The progress of the reaction in the presence of the acid catalyst reaches 97% after 1 h, which shows that the presence of the catalyst increases the reaction rate.

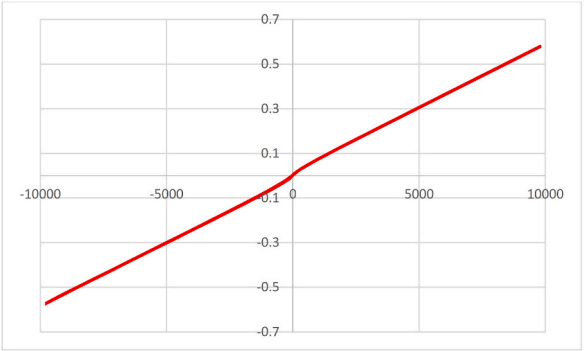

Fig. 9. VSM curves of $TiFe_2O_4@SiO_2–SO_3H$.

Table 1
Material balance calculations for the optimized yield of biodiesel in the presence of mesoporous $TiFe_2O_4@SiO_2–SO_3H$.

Entry[a]	Catalyst amount (g)	temperature (°C)	MeOH/oleic acid molar ratio (mmol/mmol)	Time (h)	Biodiesel Produced (mg)	Unreacted Material (mg)	Biodiesel yield (%)
1	–	60	9:2	8	–	–	N. R
2	0.007	60	9:1	1.5	0.098	0.46	35
3	0.01	60	9:2	1.5	0.166	0.29	59
4	0.02	60	9:2	1.5	0.273	0.48	97
5	0.03	60	9:2	1.5	0.228	0.26	81
6	0.02	25	9:2	1.5	0.141	0.27	50
7	0.02	50	9:2	1.5	0.186	0.22	66
8	0.02	60	8:2	1.5	0.163	0.38	58
9	0.02	60	11:2	1.5	0.180	0.25	64
10	0.02	60	13:2	1.5	0.211	0.23	75

Table 2
Material balance calculations for the optimized yield of biodiesel in the presence of mesoporous $TiFe_2O_4@SiO_2–SO_3H$.

Entry[a]	Catalyst amount (g)	temperature (°C)	MeOH/Palmitic acid molar ratio (mmol/mmol)	Time (h)	Biodiesel Produced (mg)	Unreacted Material (mg)	Biodiesel yield (%)
1	–	70	9:2	5	–	–	N. R
2	0.07	70	9:2	1	0.089	0.46	35
3	0.01	70	9:2	1	0.153	0.29	60
4	0.02	70	9:2	1	0.251	0.48	98
5	0.03	70	9:2	1	0.212	0.26	83
6	0.02	25	9:2	1	0.158	0.27	62
7	0.02	50	9:2	1	0.179	0.22	70
8	0.02	70	8:2	1	0.128	0.38	50
9	0.02	70	11:2	1	0.161	0.25	63
10	0.02	70	13:2	1	0.210	0.23	82

[a] Isolated yield.

3. Catalyst recyclability

To investigate the recyclability of the catalyst, the palmitic acid with methanol was examined as a model reaction using 0.02 g of $TiFe_2O_4@SiO_2–SO_3H$. Using a simple magnet, the catalyst was separated and washed several times with ethanol. The reported catalyst was recovered and reused for five periods without loss of activity (Fig. 10).

Table 3 shows the catalytic activities of previously reported catalysts compared to $TiFe_2O_4@SiO_2–SO_3H$ in the esterification of oleic acid with methanol. Considering the reaction conditions, the reported catalysts show lower catalytic efficiency than the $TiFe_2O_4@SiO_2–SO_3H$ catalyst. This indicates that the $TiFe_2O_4@SiO_2–SO_3H$ catalyst is more useful in esterification reactions compared to earlier ones (Table 3).

4. Conclusion

This work reports the investigation of an efficient procedure to prepare $TiFe_2O_4@SiO_2–SO_3H$ a novel, green, magnetic catalyst. The prepared catalyst, $TiFe_2O_4@SiO_2–SO_3H$, was identified via BET, TEM, EDS, SEM, VSM, TGA, XRD, and FT-IR. The new catalyst was

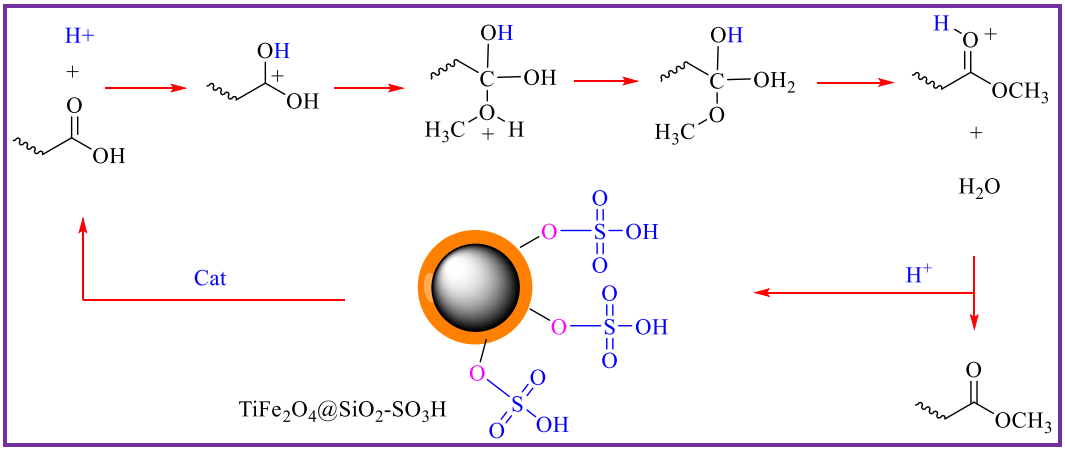

Scheme 4. Proposed Mechanism for biodiesel in this presence of $TiFe_2O_4@SiO_2–SO_3H$.

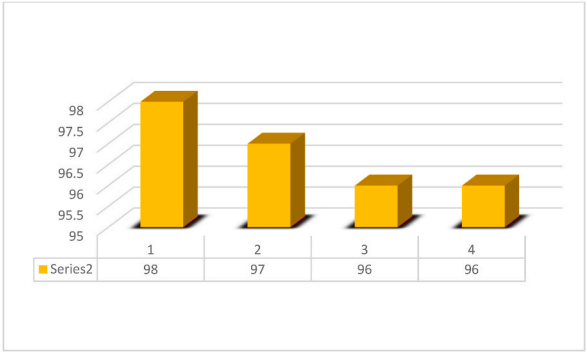

Fig. 10. Recyclability of $TiFe_2O_4@SiO_2–SO_3H$.

Table 3
Comparison of the catalytic efficiency of reported catalysts with prepared $TiFe_2O_4@SiO_2–SO_3H$ catalyst in the esterification of oleic acid with methanol.

Entry	Catalyst	Reaction	Time (mine)	Yield (%)	Ref
1	30% SiW11/MCM-41	Oleic acid + Methanol	1h	30	[26]
2	PCs–SO_3H	Oleic acid + Methanol	2h	70	[27]
3	F^--SO_4^{2-}/MWCNTs	Oleic acid + Methanol	6h	90	[28]
4	ZrFe-SA-SO_3H	Oleic acid + Methanol	4h	92	[29]
5	Na-Q-3T	Oleic acid + Methanol	2h	60	[30]
6	$TiFe_2O_4@SiO_2–SO_3H$	Oleic acid + Methanol	3h	98	This work

used for the synthesis of the esterification reactions. Moreover, this new $TiFe_2O_4@SiO_2–SO_3H$ can be easily prepared from commercially available materials. Also, it can be mentioned good catalytic activity, easy separation by an external magnet, and reusability of the introduced catalyst.

Data availability

All data generated or analyzed during this study are included in this published article [and its supplementary information files].

CRediT authorship contribution statement

Mohanad Yakdhan Saleh: Data curation, Conceptualization. **Ahmed Kareem Obaid Aldulaimi:** Project administration, Methodology, Investigation, Funding acquisition. **Shakir Mahmood Saeed:** Funding acquisition, Formal analysis. **Ayat Hussein Adhab:** Writing – review & editing, Writing – original draft, Validation.

Declaration of competing interest

The authors declare the following financial interests/personal relationships which may be considered as potential competing interests: Declaration of Competing Interest The authors declare that they have no known competing financial interests or personal relationships that could have appeared to influence the work reported in this paper. If there are other authors, they declare that they have no known competing financial interests or personal relationships that could have appeared to influence the work reported in this paper.

Acknowledgment

This work was funded by the Researchers supporting the project, College of Food Sciences, Al-Qasim Green University, Babylon, Iraq.

Appendix A. Supplementary data

Supplementary data to this article can be found online at https://doi.org/10.1016/j.heliyon.2024.e26286.

References

[1] C. Prabhu, B. Navaneetha Krishnan, T. Prakash, V. Rajasekar, D. Balasubramanian, V.V. Le, N.V. Linh Le, P.Q. Phong Nguyen, V.N. Nguyen, Biodiesel unsaturation and the synergic effects of hydrogen sharing rate on the characteristics of a compression ignition engine in dual-fuel mode, Fuel 334 (2023) 126699, https://doi.org/10.1016/j.fuel.2022.126699.
[2] M. Bayraktar, M. Pamik, M. Sokukcu, O. Yuksel, A SWOT-AHP Analysis on Biodiesel as an Alternative Future Marine Fuel, Clean Technologies and Environmental Policy, 2023, https://doi.org/10.1007/s10098-023-02501-7.
[3] Y. Zou, Y. Zhang, X. Liu, H. Zhang, Solvent-free synthetic Fe3O4@zif-8 coated lipase as a magnetic-responsive pickering emulsifier for interfacial biocatalysis, Catal. Lett. 150 (2020) 3608–3616, https://doi.org/10.1007/s10562-020-03240-w.
[4] H. Zhao, Z. Chen, L. Tao, X. Zhu, M. Lan, Z. Li, In vitro toxicity evaluation of ultra-small MFe2O4 (M = Fe, Mn, Co) nanoparticles using A549 cells, RSC Adv. 5 (2015) 68454–68460, https://doi.org/10.1039/c5ra11013k.
[5] T. Sathish, K. Muthukumar, A. Abdulwahab, M. Rajasimman, R. Saravanan, K. Balasankar, Enhanced waste cooking oil biodiesel with Al2O3 and MWCNT for CI engines, Fuel 333 (2023) 126429, https://doi.org/10.1016/j.fuel.2022.126429.
[6] H.R. Ong, M.R. Khan, M.N.K. Chowdhury, A. Yousuf, C.K. Cheng, Synthesis and characterization of CuO/C catalyst for the esterification of free fatty acid in rubber seed oil, Fuel 120 (2014) 195–201, https://doi.org/10.1016/j.fuel.2013.12.015.
[7] I. Tankov, Z. Mustafa, R. Nikolova, A. Veli, R. Yankova, Biodiesel (methyl oleate) synthesis in the presence of pyridinium and aminotriazolium acidic ionic liquids: kinetic, thermodynamic studies, Fuel 307 (2022), https://doi.org/10.1016/j.fuel.2021.121876.
[8] Z. Cai, Y. Wang, Y. Cao, P. Yu, Y. Ding, Y. Ma, Y. Zheng, K. Huang, L. Jiang, Direct production of isomerized biodiesel over MoS2/ZrPOx under solvent-free conditions, Fuel 337 (2023) 127175, https://doi.org/10.1016/j.fuel.2022.127175.
[9] N. Jeyakumar, D. Balasubramanian, M. Sankaranarayanan, K. Karuppasamy, M. Wae-Hayee, V.V. Le, V.D. Tran, A.T. Hoang, Using Pithecellobium Dulce seed-derived biodiesel combined with Groundnut shell nanoparticles for diesel engines as a well-advised approach toward sustainable waste-to-energy management, Fuel 337 (2023) 127164, https://doi.org/10.1016/j.fuel.2022.127164.
[10] M. Helmi, M. Ghadiri, K. Tahvildari, A. Hemmati, Biodiesel synthesis using clinoptilolite-Fe3O4-based phosphomolybdic acid as a novel magnetic green catalyst from salvia mirzayanii oil via electrolysis method: optimization study by Taguchi method, J. Environ. Chem. Eng. 9 (2021), https://doi.org/10.1016/j.jece.2021.105988.
[11] C. Jin, J. Wei, B. Chen, X. Li, D. Ying, L. Gong, W. Fang, Effect of nanoparticles on diesel engines driven by biodiesel and its blends: a review of 10 years of research, Energy Convers. Manag. 291 (2023) 117276, https://doi.org/10.1016/j.enconman.2023.117276.
[12] B. Jyoti Bora, P. Sharma, B. Deepanraj, Ü. Ağbulut, Investigations on a novel fuel water hyacinth biodiesel and Hydrogen-Powered engine in Dual-Fuel Model: optimization with I-optimal design and desirability, Fuel 345 (2023) 128057, https://doi.org/10.1016/j.fuel.2023.128057.
[13] Z. Cao, A. Duan, Z. Zhao, J. Li, Y. Wei, G. Jiang, J. Liu, A simple two-step method to synthesize the well-ordered mesoporous composite Ti-FDU-12 and its application in the hydrodesulfurization of DBT and 4,6-DMDBT, J. Mater. Chem. A 2 (2014) 19738–19749, https://doi.org/10.1039/C4TA03691C.
[14] K. Hasan, R.G. Joseph, S.P. Patole, R.A. Al-Qawasmeh, Development of magnetic Fe3O4-chitosan immobilized Cu(II) Schiff base catalyst: an efficient and reusable catalyst for microwave assisted one-pot synthesis of propargylamines via A3 coupling, Catal. Commun. 174 (2023) 106588, https://doi.org/10.1016/j.catcom.2022.106588.
[15] M.R. Anizadeh, M. Torabi, M.A. Zolfigol, M. Yarie, Catalytic application Fe3O4@SiO2@(CH2)3-urea-dithiocarbamic acid for the synthesis of triazole-linked pyridone derivatives, J. Mol. Struct. 1277 (2023) 134885, https://doi.org/10.1016/j.molstruc.2022.134885.
[16] H.A. Ismail, R.R. Abed, Synthesis, characterization, and biological activity assessment of new metal complexes of Schiff bases produced from benzoin, Al-Kitab Journal for Pure Sciences 7 (2023) 27–41, https://doi.org/10.32441/kjps.07.01.p3.
[17] M. Priyadarshini, A. Ahmad, M.M. Ghangrekar, Efficient upcycling of iron scrap and waste polyethylene terephthalate plastic into Fe3O4@C incorporated MIL-53(Fe) as a novel electro-Fenton catalyst for the degradation of salicylic acid, Environ. Pollut. 322 (2023) 121242, https://doi.org/10.1016/j.envpol.2023.121242.
[18] I. Fatimah, I. Yanti, H.K. Wijayanti, G.D. Ramanda, S. Sagadevan, M. Tamyiz, R. Doong, One-pot synthesis of Fe3O4/NiFe2O4 nanocomposite from iron rust waste as reusable catalyst for methyl violet oxidation, Case Studies in Chemical and Environmental Engineering 8 (2023) 100369, https://doi.org/10.1016/j.cscee.2023.100369.
[19] S. Lalhmangaihzuala, Z.T. Laldinpuii, V. Khiangte, G. Lallawmzuali, K. Vanlaldinpuia Thanhmingliana, Orange peel ash coated Fe3O4 nanoparticles as a magnetically retrievable catalyst for glycolysis and methanolysis of PET waste, Adv. Powder Technol. 34 (2023) 104076, https://doi.org/10.1016/j.apt.2023.104076.
[20] S. Zhang, Y. Shang, J. Wang, H. Chen, Y. Xiong, H. Zhang, Study on the construction of char-supported NiFe-NiFe2O4 catalyst and its catalytic cracking mechanism of biomass tar under relative low temperature, Fuel 346 (2023) 128412, https://doi.org/10.1016/j.fuel.2023.128412.
[21] H. Abed, M. Al-Jewaree, O. Adil M. Ali, An experimentally investigate the effect of physical properties on the production of lubricating materials from crude oils, Al-Kitab Journal for Pure Sciences 3 (2022) 30–47, https://doi.org/10.32441/kjps.03.01.p3.
[22] Y. Zong, L. Zhao, J. Feng, T. Wei, Y. Ren, C. Jiang, Activation of peroxymonosulfate by a magnetic Co doped NiFe2O4 catalyst for efficient Bisphenol A degradation in water, J. Taiwan Inst. Chem. Eng. 147 (2023) 104930, https://doi.org/10.1016/j.jtice.2023.104930.

[23] J. Yang, W. Cong, Z. Zhu, Z. Miao, Y.-T. Wang, M. Nelles, Z. Fang, Microwave-assisted one-step production of biodiesel from waste cooking oil by magnetic bifunctional SrO–ZnO/MOF catalyst, J. Clean. Prod. 395 (2023) 136182, https://doi.org/10.1016/j.jclepro.2023.136182.
[24] F. Kalantari, H. Esmailipour, H. Ahankar, A. Ramazani, H. Aghahosseini, O. Kaszubowski, K. Ślepokura, SO3H-Functionalized Epoxy-Immobilized Fe3O4 Core–Shell Magnetic Nanoparticles as an Efficient, Reusable, and Eco-Friendly Catalyst for the Sustainable and Green Synthesis of Pyran and Pyrrolidinone Derivatives, ACS Omega, 2023, https://doi.org/10.1021/acsomega.3c01068.
[25] S. Asiri, M. Sertkol, H. Gungunes, M. Amir, D. Manikandan, I. Ercan, A. Baykal, The temperature effect on magnetic properties of NiFe2O4 nanoparticles, J. Inorg. Organomet. Polym. Mater. 28 (2018), https://doi.org/10.1007/s10904-018-0813-z.
[26] A. Patel, N. Narkhede, Biodiesel synthesis via esterification and transesterification over a new heterogeneous catalyst comprising lacunary silicotungstate and MCM-41, Catal. Sci. Technol. 3 (2013) 3317–3325, https://doi.org/10.1039/C3CY00591G.
[27] L.H. Tamborini, M.E. Casco, M.P. Militello, J. Silvestre-Albero, C.A. Barbero, D.F. Acevedo, Sulfonated porous carbon catalysts for biodiesel production: clear effect of the carbon particle size on the catalyst synthesis and properties, Fuel Process. Technol. 149 (2016) 209–217, https://doi.org/10.1016/j.fuproc.2016.04.006.
[28] Q. Shu, W. Zou, J. He, H. Lesmana, C. Zhang, L. Zou, Y. Wang, Preparation of the F−-SO42-/MWCNTs catalyst and kinetic studies of the biodiesel production via esterification reaction of oleic acid and methanol, Renew. Energy 135 (2019) 836–845, https://doi.org/10.1016/j.renene.2018.12.067.
[29] Y.-T. Wang, X.-X. Yang, J. Xu, H.-L. Wang, Z.-B. Wang, L. Zhang, S.-L. Wang, J.-L. Liang, Biodiesel production from esterification of oleic acid by a sulfonated magnetic solid acid catalyst, Renew. Energy 139 (2019) 688–695, https://doi.org/10.1016/j.renene.2019.02.111.
[30] N. Kondamudi, S.K. Mohapatra, M. Misra, Quintinite as a bifunctional heterogeneous catalyst for biodiesel synthesis, Appl. Catal. Gen. 393 (2011) 36–43, https://doi.org/10.1016/j.apcata.2010.11.025.